Article

Evaluation of Anticancer and Anti-Inflammatory Activities of Some Synthetic Rearranged Abietanes

Mustapha Ait El Had [1,†], Houda Zentar [1,2,†], Blanca Ruiz-Muñoz [2], Juan Sainz [2,3], Juan J. Guardia [1], Antonio Fernández [1], José Justicia [1], Enrique Alvarez-Manzaneda [1], Fernando J. Reyes-Zurita [2,*] and Rachid Chahboun [1,*]

1   Departamento de Química Orgánica, Facultad de Ciencias, Instituto de Biotecnología, Universidad de Granada, 18071 Granada, Spain; mustapha.aitelhad20@gmail.com (M.A.E.H.); zentarhouda@correo.ugr.es (H.Z.); pepojaen@hotmail.com (J.J.G.); ajfvargas@ugr.es (A.F.); jjusti@ugr.es (J.J.); eamr@ugr.es (E.A.-M.)
2   Departamento de Bioquímica y Biología Molecular I, Facultad de Ciencias, Universidad de Granada, 18071 Granada, Spain; blancaruiz_@uma.es (B.R.-M.); jsainz@ugr.es (J.S.)
3   Centre for Genomics and Oncological Research: Pfizer, Genomic Oncology Area, GENYO, University of Granada, Andalusian Regional Government, PTS Granada, 18016 Granada, Spain
*   Correspondence: ferjes@ugr.es (F.J.R.-Z.); rachid@ugr.es (R.C.); Fax: +34-958-248-437 (R.C.)
†   These authors contributed equally to this work.

Abstract: Synthesis of the rearranged abietane diterpenes pygmaeocins C and D, viridoquinone, saprorthoquinone, and 1-deoxyviroxocine has been successfully achieved. The anticancer and anti-inflammatory activities of selected orthoquinonic compounds **5**, **7**, **13**, and **19**, as well as pygmaeocin C (**17**), were evaluated for the first time. The antitumor properties were assessed using three cancer cell lines: HT29 colon cancer cells, Hep G2 hepatocellular carcinoma cells, and B16-F10 murine melanoma cells. Compounds **5** and **13** showed the highest cytotoxicity in HT29 cells (IC$_{50}$ = 6.69 ± 1.2 µg/mL and IC$_{50}$ = 2.7 ± 0.8 µg/mL, respectively). Cytometric studies showed that this growth inhibition involved phase S cell cycle arrest and apoptosis induction, possibly through the activation of the intrinsic apoptotic pathway. Morphological apoptotic changes, including nuclear fragmentation and chromatin condensation, were also observed. Furthermore, the anti-inflammatory activity of these compounds was evaluated on the basis of their ability to inhibit nitric oxide production on the lipopolysaccharide activated RAW 264.7 macrophage cell line. Although all compounds showed high anti-inflammatory activity, with percentages between 40 and 100%, the highest anti-inflammatory potential was obtained by pygmaeocin B (**5**) (IC$_{50NO}$ = 33.0 ± 0.8 ng/mL). Our results suggest that due to their dual roles, this type of compound could represent a new strategy, contributing to the development of novel anticancer agents.

Keywords: rearranged abietane type; semisynthesis; antitumor activity; apoptosis; colorectal cancer; anti-inflammatory activity; nitric oxide

1. Introduction

Cancer is currently one of the most common causes of death worldwide, with its prevalence projected to reach 21 million cases by 2030 [1]. The current chemotherapeutic drugs used in cancer treatment often have severe side effects and can lead to resistance development. Thus, there is an urgent need for novel and potent antitumor agents with reduced toxicity. Natural products, which have been used for centuries to prevent and treat human diseases, offer a promising avenue for the discovery of such active compounds. The plant kingdom serves as an abundant source of bioactive compounds with exceptional therapeutic potential [2], and over 25% of approved drugs in cancer therapy are derived from natural sources [3]. Plants, the basis of traditional medicine, are instrumental in the search for chemical structures that have led to the discovery of new drugs. These

compounds, known as secondary metabolites, are synthesized by plants in response to various environmental stresses, enabling their interaction with their surroundings and contributing to their survival [4]. Notably, among these metabolites are abietanes, a vast group of diterpenes displaying a wide range of biological activities [5]. Abietanes with a phenanthrene skeleton are the most common group of this class of diterpenes. Thus, ferruginol (**1**) [6], which contains a tricyclic structure with an aromatic C-ring, is a classic example (Figure 1). Seco-abietanes with an aromatic B-ring are derivatives resulting from the loss of a methyl group on C-10. A prominent example of this peculiar group of *nor*-diterpenes is represented by tanshinone IIA (**2**), which has been shown to exert a proapoptotic function against the MCF–7 breast cancer cell line by inhibiting the downstream signaling of protein kinase C [7].
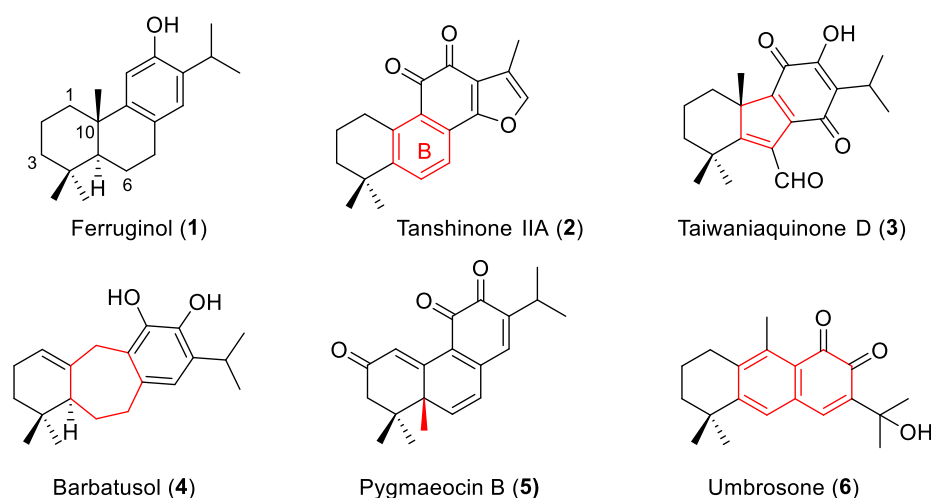

Figure 1. Examples of aromatic and rearranged abietane diterpenes (types 1–4).

On the other hand, a crucial aspect of this research is the relationship between chronic inflammation and tumor development [8], which can lead to various diseases, including cancer. As a consequence, there is a strong interest in developing novel anti-inflammatory agents with potent anticancer properties [9,10]. In line with this information, our ongoing efforts to discover new potential drugs have led us to synthesize natural abietane and rearranged abietanes and evaluate their anticancer and anti-inflammatory activities.

Rearranged abietane-type diterpenes constitute a reduced group of secondary metabolites that are structurally and biologically very interesting. According to the structures of their skeletons, they can be divided into five subgroups: Taiwaniquinone D (**3**) [11] (type 1) and barbatusol (**4**) [12] (type 2) are two examples of the rearranged abietane family. The former has a contracted B-ring of the abietane skeleton, whereas the latter has an expanded B-ring with a 9(10-20) abeo-abietane skeleton called icetexane. The other three types are exemplified by Pygmaeocin B (**5**) [13] (type 3), which is characterized by a methyl C-20 transposed from C-10 to C-5; umbrosone (**6**) [14], with a phenanthrene skeleton; and saprorthoquinone (**7**) (type 5), a 4,5-seco-abietane with an *o*-naphthoquinone structure isolated from the roots of *Salvia prionitis* [15] and exhibiting strong cytotoxicity against P388 leukemia cells [16].

Pygmaeocin B (**5**) [13] (type 3), with methyl C-20 transposed from C-10 to C-5, and umbrosone (**6**) [14] (type 4), with a phenanthrene skeleton, are two other rearranged abietanes (Figure 1). Finally, saprorthoquinone (**7**) (type 5), a bicyclic naphthoquinone with a rearranged abietane structure abietane diterpenoid, which was isolated from the roots of *Salvia prionitis* [15], exhibits strong cytotoxicity against P388 leukemia cells [16]. This last type class of rearranged abietane can undergo biological transformation to other related tricyclic metabolites, such as ceratodiol (**8**) [17,18], saprirearine (**9**) [18], microstegiol (**10**) [18], candidissiol (**11**) [18], and 1-deoxyviroxocin (**12**) [17,19,20] (Figure 2). 1-Deoxyviroxocin (**12**), with an oxocane ring, is an unusual oxygenated eight-membered

ring-type oxocane and was isolated from different natural sources such as the cones of *Taxodium distichum* L. [17], a conifer widely distributed in the southeastern United States. Furthermore, 1-deoxyviroxocin (**12**) has also been isolated from *Caryopteris incana* (Thunb.) [20] and from the roots of *Zhumeria majdae*, an endemic Iranian plant belonging to the Lamiaceae family with anti-inflammatory, antiprotozoal, and anticonvulsant properties [19].
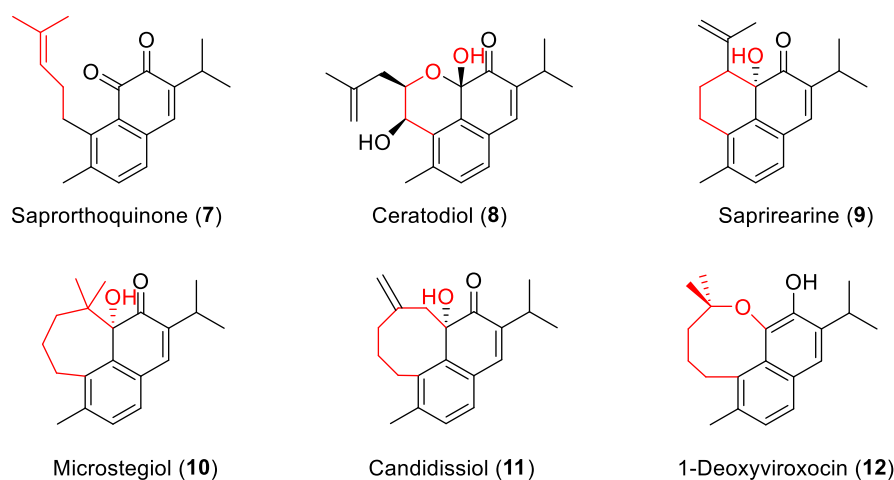

**Figure 2.** Some examples of aromatic and rearranged abietane diterpenes (type 5).

This study presents the synthesis of the natural compounds pygmaeocins B (**5**) and C (**17**), viridiquinone (**19**), saprorthoquinone (**7**), and 1-deoxyviroxocin (**12**) from ferruginol (**1**). Moreover, we conducted a biological evaluation of the natural and synthetic compounds, which include pygmaeocins B (**5**) and C (**17**), viridoquinone (**19**), saprortoquinone (**7**), and the syntetical *ortho*quinone **13**. These selected compounds were evaluated for their inhibitory activity against nitric oxide (NO) production in the lipopolysaccharide (LPS)-induced murine macrophage RAW 264.7 cell line, as well as for their antiproliferative activity against colon cancer cells (HT29), melanoma cells (B16–F10), and hepatoma cells (HepG2). Furthermore, cytometric and microscopic assays were performed on the most active compounds pygmaeocin B (**5**) and its precursor **13**.

2. Results

2.1. Chemistry

During our studies on the synthesis of abietanes, a new synthetic methodology was developed and applied to the preparation of some rearranged abietanes type 2, such as pygmaeocin B (**5**), pygmaeocin C (**17**), and viridoquinone (**19**) [21] from ferruginol (**1**). The first step involved the oxidation of **1** to orthoquinone **13** with $(PhSeO)_2O$, which after treatment with $Sc(OTf)_3$ in the presence of Ac_2O generated the derivative **14**. This compound was transformed into **16** by the action of SeO_2 under reflux in dioxane and subsequent oxidation with PDC. Deprotection of catechol **16** with conc. HCl generated pygmaeocin C (**17**), which was easily oxidized to pygmaeocin B (**5**) using Ag_2O (see Scheme 1).

Next, viridiquinone (**19**) was successfully obtained in two steps from orthoquinone **13** by isomerization with conc. H_2SO_4 and subsequent oxidation with SeO_2 at reflux in dioxane (see Scheme 2).
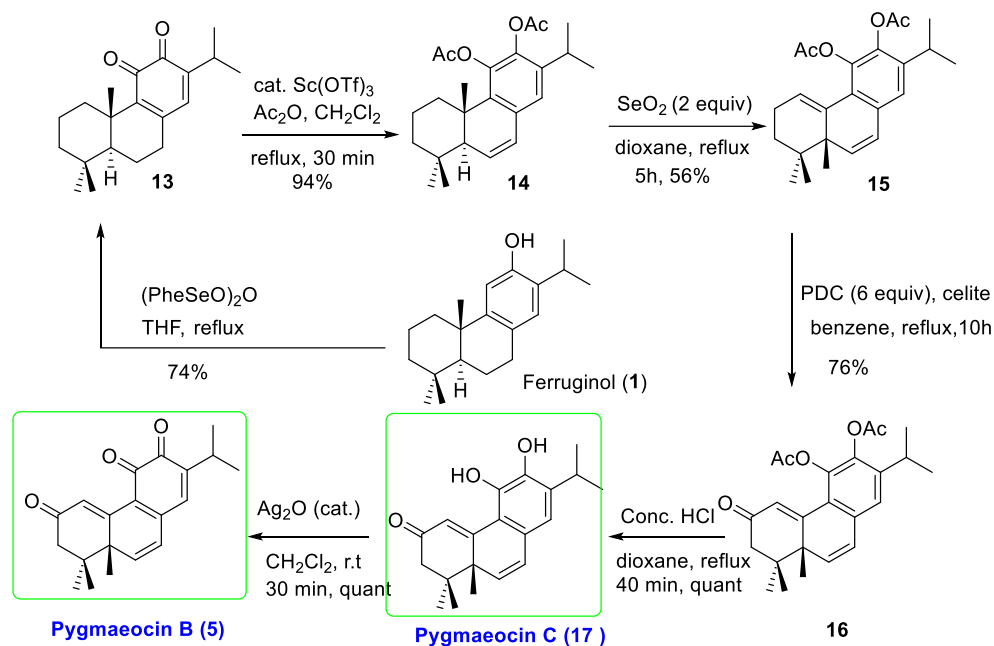
Scheme 1. Synthesis of pygmaeocins B (**5**) and C (**17**) from ferruginol (**1**).
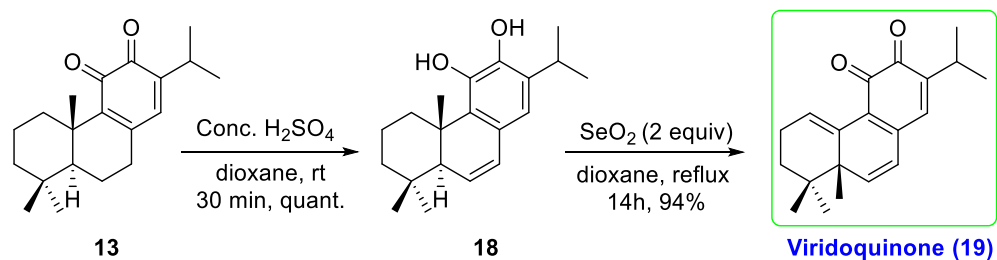
Scheme 2. Synthesis of viridoquinone (**19**) from abietane orthoquinone **13**.

Treatment of catechol **18** with one equivalent of SeO$_2$ in the presence of a catalytic amount of H$_2$SO$_4$ surprisingly led to saprorthoquinone (**7**), a rearranged abietane-type 5 previously synthesized in eight steps from ferruginol methyl ether, with an overall yield of 24% [22]. When this reaction was carried out with two equivalents of SeO$_2$ and 1-eq of H$_2$SO$_4$, aldehyde **20** was obtained after 15 min of refluxing in dioxane. The treatment of orthoquinone **13** with SeO$_2$ and conc. H$_2$SO$_4$ under stoichiometric amounts leads directly to saprorthoquinone (**7**) after 20 min with a good yield. Thus, the synthesis has been completed in only two steps starting from ferruginol (**1**), with an overall yield of 60% (see Scheme 3).

Finally, the treatment of catechol **18** with two equivalents of SeO$_2$ at reflux in dioxane in the absence of acid yielded hydroxyenone **21**, which was completely transformed into 1-deoxyviroxocin (**12**) after reaction with I$_2$/PPh$_3$ for 10 min at room temperature (Scheme 3). Therefore, the first synthesis of 1-deoxyviroxocin (**12**) from ferruginol (**1**) was carried out in only four steps. The NMR spectroscopic data of **12** were compared with those described in the literature (see SI). In general, all the obtained signals agreed with the published data, and there were hardly any significant deviations; therefore, the structure of 1-deoxyviroxocin (**12**) was confirmed.
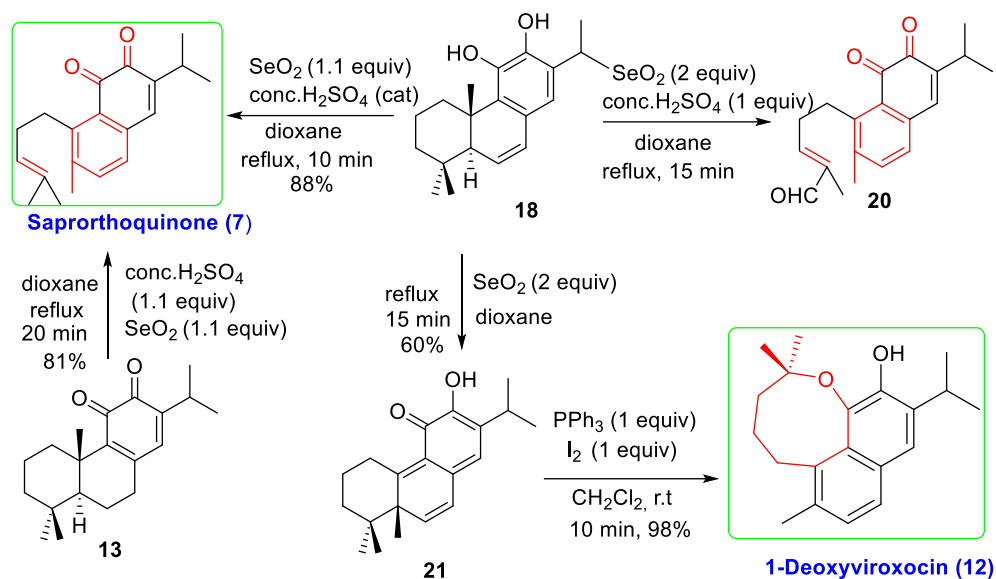
Scheme 3. Synthesis of saprorthoquinone (**7**) and 1-deoxyviroxocin (**12**) from catechol **18**.

2.2. Anticancer Activity

2.2.1. Cell Viability Assay

In this study, we employed the MTT (3-(4,5-dimethyl thiazol-2-yl)-2,5-diphenyltetrazolium bromide) colorimetric assay to evaluate the cytotoxic activity of selected abietanes (compounds **5**, **7**, **13**, **17**, and **19**) against three tumor cell lines: human colon adenocarcinoma (HT29), human hepatocarcinoma (HepG2), and murine melanoma (B16–F10). The MTT assay relied on the conversion of MTT to formazan by viable cells, with the formazan concentration proportional to the number of viable cells. The concentrations required for 50 and 80% growth inhibition (IC_{50} and IC_{80}) were determined for each compound.

After 72 h of treatment, all tested compounds demonstrated a dose-dependent decrease in cell viability. Among the abietanes, compound **13**, which serves as the precursor for the synthesis of the selected rearranged abietanes, exhibited the highest cytotoxicity in all three cell lines, with IC_{50} values ranging from 2.67 to 5.58 μg/mL and IC_{80} values in the range of 5.19 to 7.67 μg/mL. Furthermore, pygmaeocin B (**5**) demonstrated substantial cytotoxic activity against the HT29 and HepG2 cell lines, with IC_{50} concentrations of 6.69 and 8.98 μg/mL, respectively. In contrast, Viridoquinone (**19**) displayed much lower toxicity in these two cell lines, with IC_{50} values up to 23 and 14 times higher than that of precursor compound **13**, respectively. The remaining diterpenoids (**5**, **7**, and **17**) exhibited comparable effects on cell growth in the HT29 and HepG2 cell lines (Table 1).

Interestingly, the cytotoxic response of B16–F10 melanoma cell line to the compounds differed significantly. In this case, Viridoquinone (**19**) and Saprorthoquinone (**7**) exhibited high cytotoxicity, with IC_{50} values of 6.42 and 6.89 μg/mL, respectively. However, Pygmaeocin B (**5**) did not significantly reduce the growth of B16–F10 cells, with an IC_{50} value 3.5 times higher than that of compound **13**. Based on their promising cytotoxic activity, pygmaeocin B (**5**) and synthetic orthoquinone **13** were selected for further investigation of the mechanisms involved in HT29 colon adenocarcinoma cell growth inhibition. The dose–response curves for these compounds are illustrated in Figure 3.

These findings reveal the potential of compounds **5** and **13** as plausible candidates for future development in cancer therapy and underscore the importance of further research to elucidate their mechanisms of action in tumor cells. These products were selected for the percentage of apoptosis determination, cell cycle distribution, and mitochondrial membrane potential measurements. All these assays were realized in the HT29 colon adenocarcinoma cell line by flow cytometry analysis in a fluorescence-activated cell sorter.

Table 1. Growth-inhibitory effects of the tested compounds (**5**, **7**, **13**, **17**, and **19**) on the three cancer cell lines.

Cell Line	Compound	IC$_{50}$ (µg/mL)	IC$_{80}$ (µg/mL)
HT29	Pygmaeocin B (**5**)	6.69 ± 1.18	9.73 ± 1.18
	Saprorthoquinone (**7**)	7.82 ± 0.17	10.62 ± 0.28
	Pygmaeocin C (**17**)	15.28 ± 0.71	24.36 ± 2.65
	Viridoquinone (**19**)	60.52 ± 0.28	74.65 ± 1.53
	Precursor (**13**)	2.67 ± 0.82	5.19 ± 0.68
HepG2	Pygmaeocin B (**5**)	8.99 ± 1.12	11.41 ± 1.08
	Saprorthoquinone (**7**)	21.16 ± 2.26	29.12 ± 0.21
	Pygmaeocin C (**17**)	38.75 ± 1.55	73.53 ± 2.06
	Viridoquinone (**19**)	76.27 ± 2.14	100.57 ± 3.47
	Precursor (**13**)	5.58 ± 0.93	7.67 ± 0.80
B16-F10	Pygmaeocin B (**5**)	13.63 ± 0.14	14.04 ± 0.08
	Saprorthoquinone (**7**)	6.89 ± 0.37	8.02 ± 0.52
	Pygmaeocin C (**17**)	10.11 ± 1.81	26.61 ± 4.82
	Viridoquinone (**19**)	6.42 ± 0.35	9.14 ± 0.38
	Precursor (**13**)	4.14 ± 0.25	5.41 ± 0.25
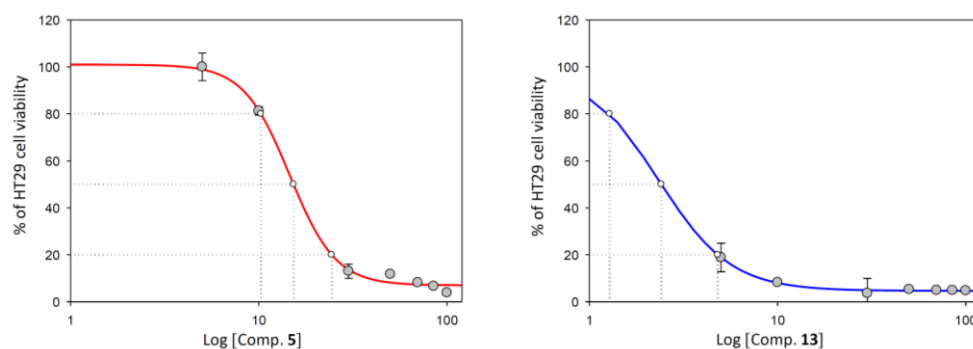
Figure 3. Sigmoidal curves of cytotoxicity of Pygmaeocin B (**5**) and its precursor (**13**) on HT29 colon adenocarcinoma cells. The percentage of relative viability (with respect to the untreated control) is shown against the logarithm of the dose of the used product. Each point represents the mean ± standard deviation, from three replicates for each concentration.

2.2.2. Cell Cycle Arrest and Distribution

Flow cytometry was employed to assess the impact of compounds **5** and **13** on the cell cycle profiles of HT29 cells after 72 h of treatment; by using propidium iodide (PI) incorporation, whose fluorescence directly correlated with DNA content, we analyzed the distribution of cells in different cell cycle phases. The DNA histogram analysis (Figure 4) demonstrated that both compounds induced cell cycle arrest in the S phase.

Orthoquinone **13** caused a significant increase in the cell population in the S phase, up by 10% compared with the control (untreated cells), regardless of the administered dose. This increase was accompanied by a decrease in the cell populations in the G0/G1 and G2/M phases. On the other hand, Pygmaeocin B (**5**) exhibited a more pronounced arrest of the cell cycle in the S phase at IC$_{80}$ doses compared with IC$_{50}$ doses, leading to increases of 4% and 10%, respectively, compared with the control. However, the changes in the cell number in the G2/M phase were not significant.

These results provided information about the impact of compounds **5** and **13** on the cell cycle of HT29 cells, showing their potential as cytostatic agents, although these results could also be related to the cell cycle arrest that accompanies apoptosis induction. Future studies will be needed to clarify this point.
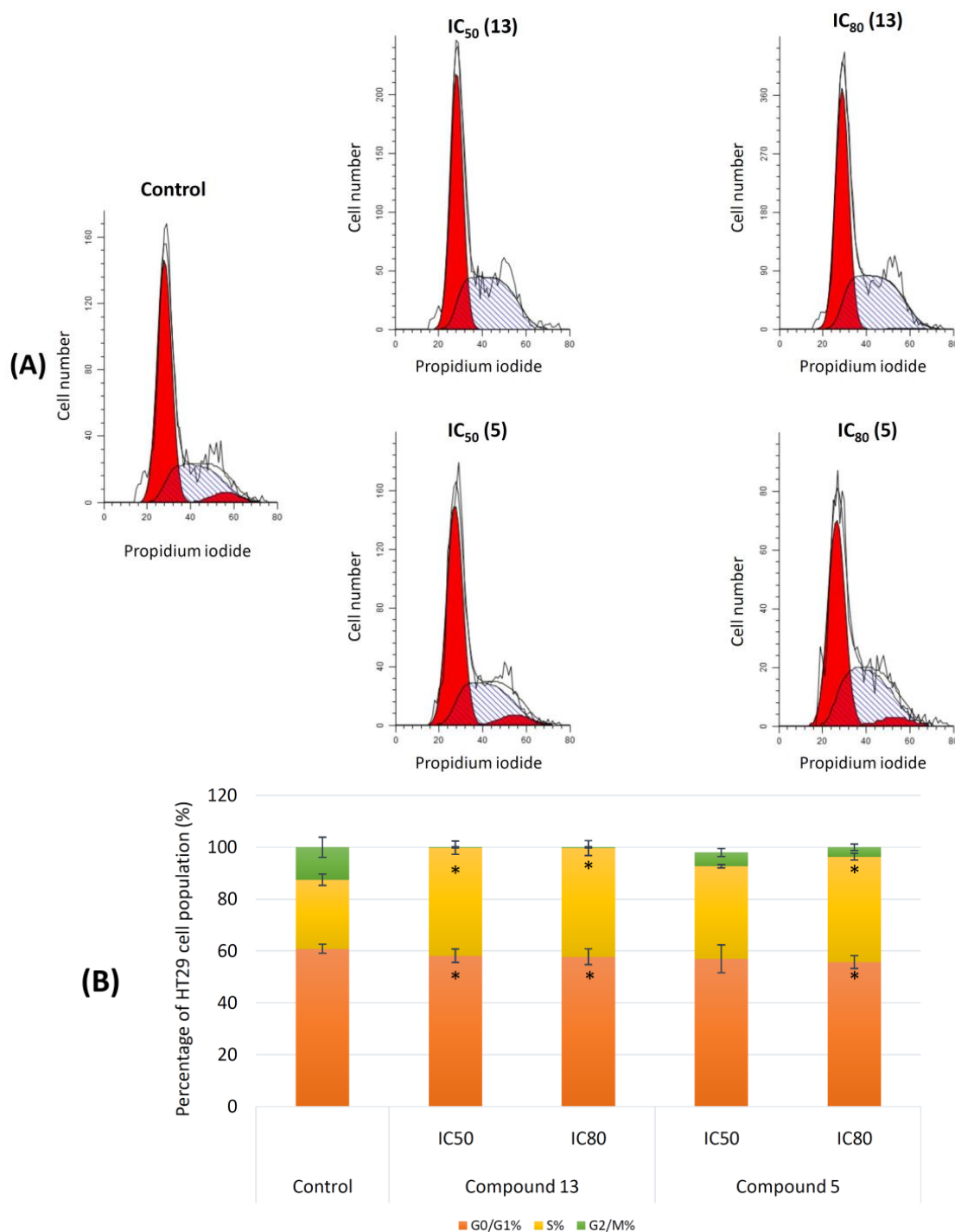
Figure 4. Flow cytometric analysis of the cell cycle of HT29 colon carcinoma cells with or without (control) compounds **5** and **13** at IC_{50} and IC_{80} concentrations for 72 h. (**A**) Representative histograms obtained by FACS. (**B**) Increase in the percentage of cells in each phase of the cell cycle with respect to the control of untreated cells. Values represent the mean $\pm$ standard deviation from at least two experiments in triplicates. Key: $p < 0.05$ (*), $p \leq 0.01$ (**), and $p \leq 0.001$ (***) with respect to untreated control cells.

2.2.3. Induction of Apoptosis in Tumor Cell Lines

During the apoptosis process, the loss of the cytoplasmic membrane asymmetry occurs, caused by the translocation of phosphatidylserine (PS) from the leaflet of the internal membrane to the external membrane to be recognized by macrophage cells [23].

The exposed PS is recognized by annexin V phospholipid-binding protein, which binds to and fluorescently labels apoptotic cells.

To further investigate the potential mechanisms underlying the cytotoxic and cytostatic effects of compounds **5** and **13** on HT29 cells, Annexin V–FITC/PI double staining along with flow-activated cell sorter (FACS) cytometry analysis was employed for determinate apoptosis induction. This assay allowed for the distinction of different cell populations, including normal cells (Annexin V− PI−), early apoptotic cells (Annexin V+ PI−), late apoptotic cells (Annexin V+ PI+), and necrotic cells (Annexin V− PI+).

These assays on the HT29 cell line were conducted 72 h after treatment with the selected rearranged abietanes at their corresponding IC_{50} and IC_{80} concentrations. The results revealed significant apoptotic effects induced by both compounds on HT29 cells compared with the control group. Orthoquinone **13** induced apoptosis in 18% (6% early apoptosis and 12% late apoptosis) and 21% (7% early apoptosis and 14% late apoptosis) of the cell population at the IC_{50} and IC_{80} concentrations, respectively, as opposed to 9% of apoptotic cells in the control group (Figure 5).
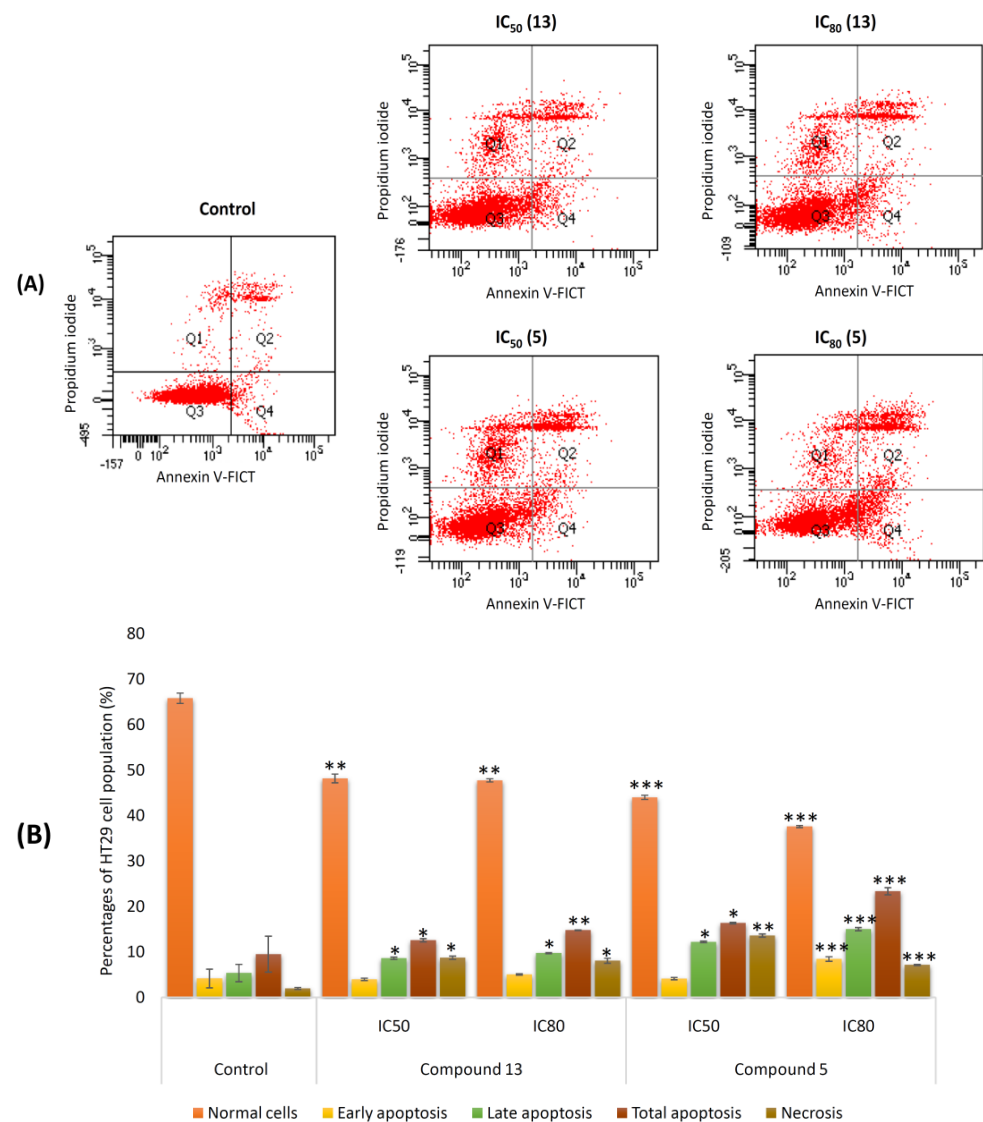

Figure 5. Annexin V−FITC/IP stained flow cytometric analysis of HT29 colon carcinoma cells with or without (control) compounds **5** and **13** at IC_{50} and IC_{80} concentrations for 72 h. (**A**) Representative flow cytometry diagrams. (**B**) Bar charts of the percentage of apoptotic (early, late, and total) and necrotic HT29 cells. Values represent the mean ± standard deviation of at least two experiments in triplicates. Key: $p < 0.05$ (*), $p \leq 0.01$ (**), and $p \leq 0.001$ (***) with respect to untreated control cells.

Regarding pygmaeocin B (**5**), apoptosis induction was dose dependent, with 22% of total apoptosis at the IC_{50} concentration (5% early apoptosis and 17% late apoptosis), increasing to 35% at the IC_{80} concentration (12% early apoptosis and 23% late apoptosis). The percentage of necrotic cells was relatively high especially with treatment with compound **5** at the IC_{50} concentration compared with the control (15% vs. 3% for the control). Our results demonstrate the potent apoptotic effects of compounds **5** and **13** on HT29 cells. Further investigations are needed to elucidate the specific apoptotic trigger mechanisms involved in the apoptotic effects.

2.2.4. Effects on Mitochondrial Membrane Potential (MMP)

Apoptotic effects induced by anticancer agents can be mediated through two major pathways: intrinsic and extrinsic apoptotic pathways. The intrinsic pathway involves the disruption of the mitochondrial membrane and changes in the mitochondrial membrane potential (MMP), while the extrinsic pathway leads to apoptosis without initial MMP alterations. To investigate the apoptotic responses of the HT29 cells treated with compounds **5** and **13**, the MMP changes were analyzed using flow cytometry staining with rhodamine 123 (Rh123) and IP after 72 h of treatment at IC_{50} and IC_{80} concentrations. The results showed that both orthoquinone **13** and pygmaeocin B (**5**) produced changes in the mitochondrial membrane potential with respect to the control (untreated cells) (Figure 6). Treatment with precursor **13** caused a decrease in positive Rh123-stained HT29 cells of around 40% at the IC_{50} concentration and 57% at the IC_{80} concentration, with the consequent increase in the negative cell population. Pygmaeocin B (**5**) caused a greater loss of membrane potential, with 54 and 61% decreases in Rh123+ cells with regard to the untreated control at IC_{50} and IC_{80} concentrations, respectively. This finding suggests that the apoptosis induction of compounds **5** and **13** in HT29 cells occurs through the activation of the intrinsic apoptotic pathway. Further investigations are necessary to elucidate the detailed molecular mechanisms underlying their apoptotic effect.
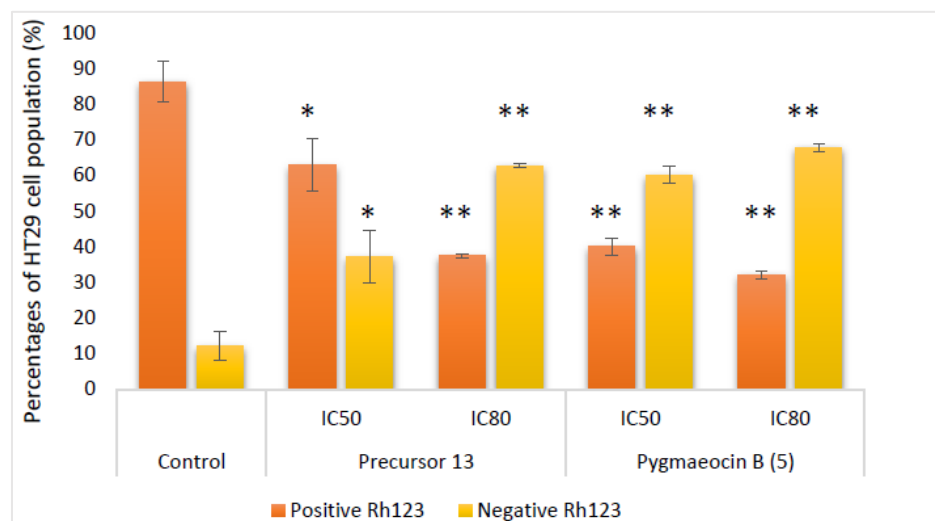

Figure 6. The effect of treatment of compounds **5** and **13** for 72 h at IC_{50} and IC_{80} concentrations on the mitochondrial membrane potential of HT29 cells. Flow cytometry analysis is shown as the percentage of cells positive and negative for Rh123 staining. Data are expressed as the mean $\pm$ standard deviation of at least two experiments in triplicates. Key: $p < 0.05$ (*), $p \leq 0.01$ (**), and $p \leq 0.001$ (***) with respect to untreated control cells.

2.2.5. Morphological Changes during Apoptosis Hoechst Staining

To assess the apoptosis induction capacity of compounds **5** and **13** on HT29 cells, we performed Hoechst 33242 nuclear staining, a well-established method for visualizing the morphological changes associated with apoptosis. Two principal morphological characteristics can be observed in the apoptosis process, chromatin condensation and nuclei

fragmentation. Hoechst is a dye capable of penetrating cells and binding to double-stranded DNA, emitting blue light that can be visualized by using fluorescence microscopy.

After treating the colon adenocarcinoma cell line HT29 with diterpenoids **5** and **13** at IC_{50} and IC_{80} concentrations for 72 h, we examined the fluorescence images to evaluate the nuclear morphology (Figure 7). The control cells exhibited intact nuclear morphology, while a significant number of treated cells displayed apoptotic characteristics. At the IC_{50} concentration, both compounds caused the loss of normal nuclear architecture and chromatin condensation, as indicated by the higher concentration of Hoechst dye (bright blue). At the higher IC_{80} concentration, the chromatin condensation became irreversible, leading to the formation of pyknotic or contracted nuclei followed by fragmentation into apoptotic bodies (white arrow).
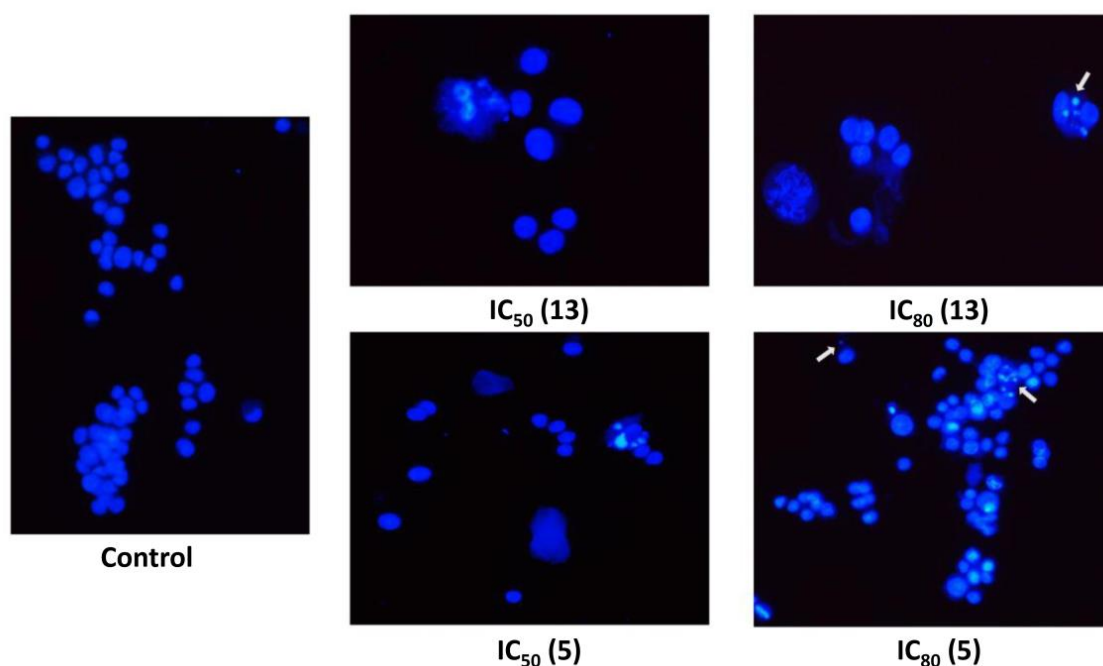

Figure 7. Fluorescence microscopy with Hoechst staining of HT29 cells in the presence or not (control) of compounds **5** and **13** at IC_{50} and IC_{80} concentrations for 72 h. White arrows indicate apoptotic bodies.

These results demonstrate that compounds **5** and **13** have remarkable apoptotic effects on HT29 cells inducing nuclear morphological changes characteristic of apoptosis. These findings support the potential use of these diterpenoids as promising agents for targeted apoptosis induction in colon adenocarcinoma cells. Further molecular studies will be necessary to confirm the underlying molecular mechanisms of the apoptotic activity of these products and to advance their potential applications in cancer therapy.

2.3. Anti-Inflammatory Activity
2.3.1. RAW 264.7 Cell Viability

To evaluate the cytotoxic effects of the synthesized abietanes (**5**, **7**, **13**, **17**, and **19**) on RAW 264.7 monocyte/macrophage murine cells and to establish sub-cytotoxic concentrations for anti-inflammatory testing, we conducted cell viability assays using the MTT method. Each compound was tested at increasing concentration levels (0–100 µg/mL), and the IC_{50} values were determined by interpolation in the sigmoidal cytotoxicity curves (Figure 8). The obtained IC_{50} values for the different abietanes were as follows: 0.14 ± 0.09 µg/mL for pygmaeocin B (**5**), 2.81 ± 0.45 µg/mL for saprorthoquinone (**7**), 6.27 ± 0.94 µg/mL for pygmaeocin C (**17**), 9.29 ± 0.35 µg/mL for viridoquinone (**19**), and 8.18 ± 1.86 µg/mL for their precursor **13**. Additionally, sub-cytotoxic concentrations corresponding to 3/4 IC_{50}, 1/2 IC_{50}, and 1/4 IC_{50} were determined and selected for subsequent anti-inflammatory as-

says, ensuring that the observed effects were specifically attributed to the anti-inflammatory properties of the compounds rather than cytotoxicity.
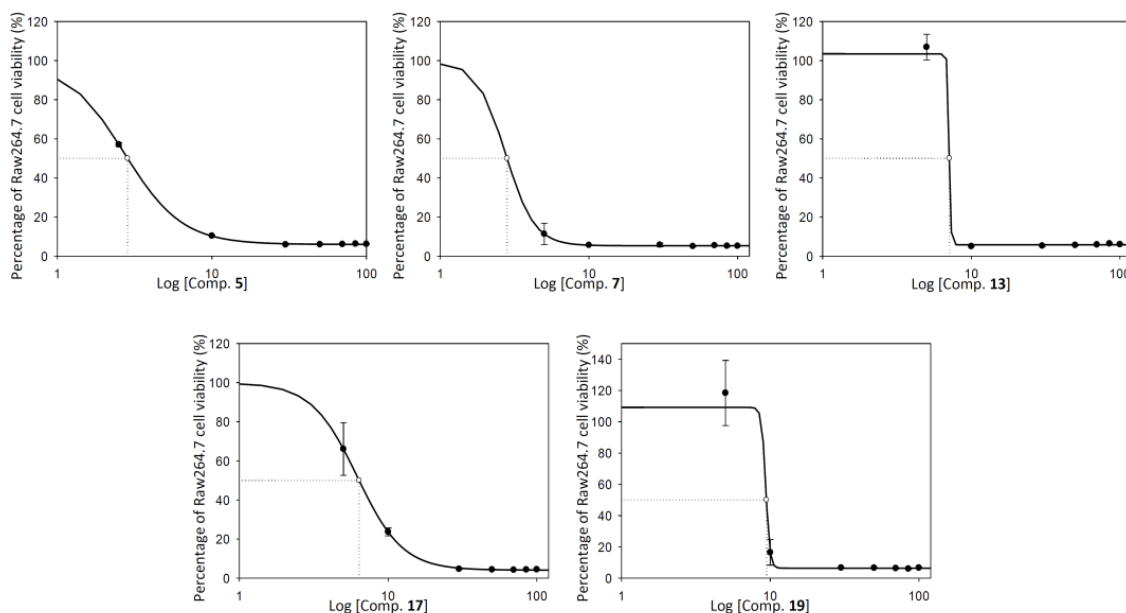

Figure 8. Cytotoxicity sigmoidal curves of abietane-type diterpenoids (**5**, **7**, **13**, **17**, and **19**) on the RAW 264.7 monocyte/macrophage line. The percentage of relative viability (concerning the untreated control) is shown against the logarithm of the dose of the product used. Each point represents the mean ± standard deviation from three replicates for each concentration.

These results demonstrate the cytotoxicity profile of synthesized abietanes on RAW 264.7 cells and provide the groundwork for investigating their potential anti-inflammatory effects at non-cytotoxic concentrations. The data support the selection of appropriate sub-cytotoxic concentrations for further anti-inflammatory experiments enabling a comprehensive evaluation of the compounds' anti-inflammatory properties.

2.3.2. Inhibition of Nitric Oxide (NO) Production

To evaluate the anti-inflammatory activity of the rearranged abietanes (**5**, **7**, **17**, and **19**) along with their precursor **13**, we conducted experiments on RAW 264.7 macrophage cells, a well-known model for screening anti-inflammatory compounds. The macrophages were stimulated with LPS to induce the maximum release of nitric oxide (NO) during the inflammatory response. Subsequently, the different compounds were incubated with the cells at sub-cytotoxic concentrations for 48 h (Figure 9). Next, we determined the concentration of nitrites in the culture medium, which was proportional to the amount of NO release.

The results demonstrated that all tested compounds exerted dose-dependent inhibition of NO release. At $3/4$ IC_{50} concentration, pygmaeocin B (**5**), saprorthoquinone (**7**), and viridoquinone (**19**) achieved 100% NO inhibition, indicating strong anti-inflammatory effects. Precursor **13** and pygmaeocin C (**17**) also significantly reduced NO release, with inhibition percentages of 99.6% and 91%, respectively. At $1/2$ IC_{50} concentration, all compounds showed strong inhibitory activity, with inhibition percentages ranging from 94 to 96%. At $1/4$ IC_{50} concentration, the rearranged abietanes and their precursor displayed moderate to good inhibition of the inflammatory process, with inhibition percentages of NO release ranging from 42 to 64%.
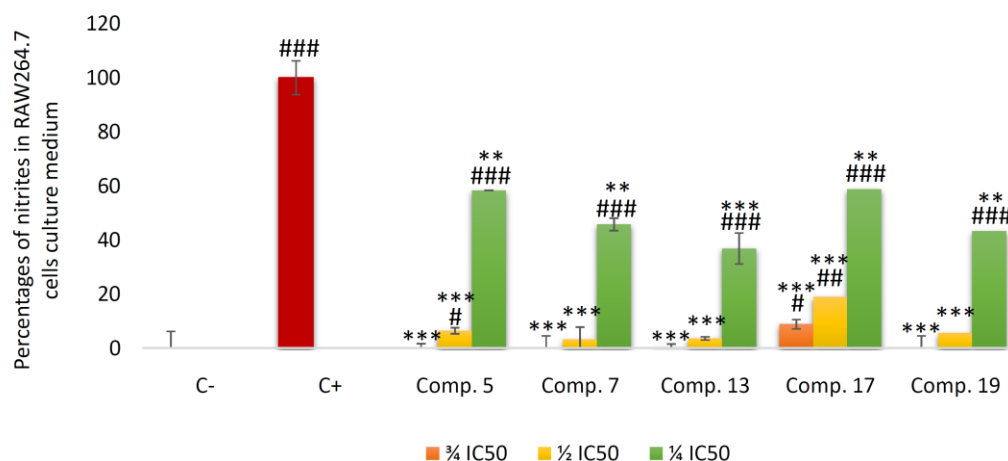
Figure 9. Effects of the rearranged abietanes and their precursors (**5**, **7**, **13**, **17**, and **19**) on nitrite release in RAW 264.7 macrophage cells. After activation of the inflammatory process, the compounds were incubated for 48 at concentrations of $^3/_4$ IC$_{50}$, $^1/_2$ IC$_{50}$, and $^1/_4$ IC$_{50}$. Data represent the mean $\pm$ SD of at least two independent experiments performed in triplicate. Key: $p < 0.05$ (#), $p \leq 0.01$ (##), $p \leq 0.001$ (###) compared with negative control; $p < 0.05$ (*), $p \leq 0.01$ (**), $p \leq 0.001$ (***) compared with positive control.

Furthermore, to provide a comprehensive anti-inflammatory characterization of the compounds, we calculated the IC$_{50\,NO}$ values at 48 h of cell incubation (Figure 10). Among the compounds, pygmaeocin B (**5**) exhibited the highest effectiveness in inhibiting NO release in RAW macrophages, with an IC$_{50\,NO}$ of 33.0 $\pm$ 0.8 ng/mL, which was 61 times lower than that of its precursor **13** (2.03 $\pm$ 0.09 µg/mL). Saprorthoquinone (**7**) and pygmaeocin C (**17**) showed IC$_{50\,NO}$ values of 1.30 $\pm$ 0.08 and 1.73 $\pm$ 0.04 µg/mL, respectively. Finally, the IC$_{50\,NO}$ value for viridoquinone (**19**) was 7.21 $\pm$ 0.9 µg/mL.
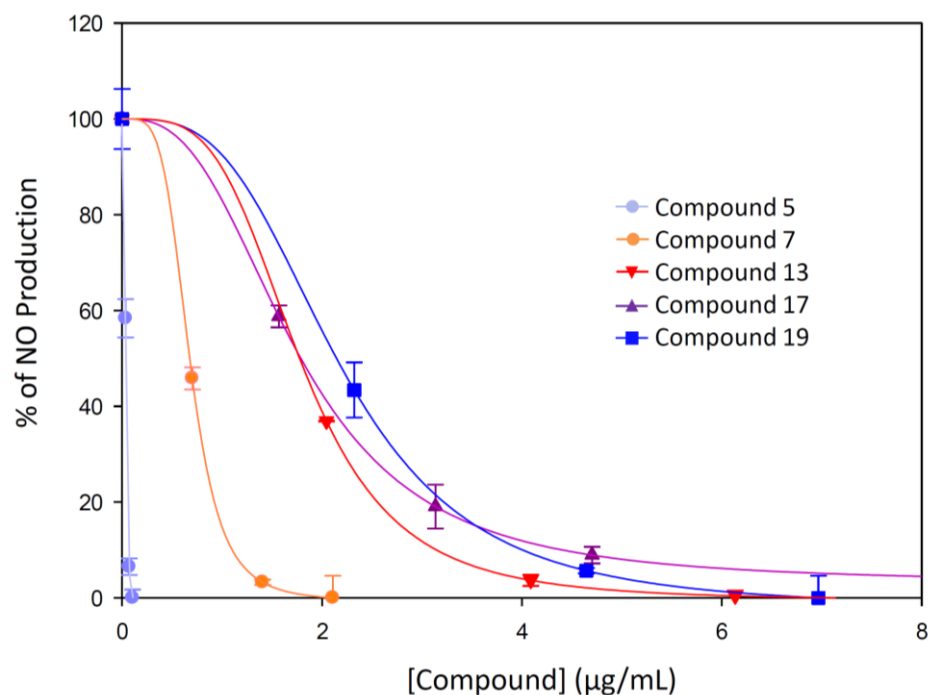

Figure 10. Sigmoidal curves of the effect of compounds (**5**, **7**, **13**, **17**, and **19**) on the release of NO in RAW 264.7 macrophage cells after 48 h of treatment. Data represent the mean $\pm$ standard deviation from three replicates.

These findings highlight the potent anti-inflammatory effects of synthetized abietanes (**5**, **7**, **17**, and **19**) and their precursor **13** on RAW 264.7 macrophage cells. The results support their potential as promising candidates for further development as anti-inflammatory agents, and their distinct mechanisms of action merit further investigation.

3. Discussion

Abietanes are a fascinating family of naturally occurring diterpenoids isolated from numerous plant species that have captured significant attention from the pharmacological community due to their diverse and intriguing biological potential. Over the past two decades, the scientific investigation of abietane and rearranged abietane-type diterpenoids has been a highly dynamic field of research. This extensive investigation has resulted in numerous publications focusing on the isolation, structural characterization, and preliminary biological studies of these compounds [24].

During our investigations, we found that the precursor, orthoquinone **13**, displayed the highest efficacy in inhibiting the proliferation of three tumor-tested cell lines. This remarkable result emphasizes the significance of modifying natural products to discover promising anticancer agents with superior bioactivity compared with their natural equivalents [25]. Structural analysis revealed that precursor **13** did not possess a rearranged abietane skeleton but presented orthoquinone functionality at C-11 and C12, which may have been responsible for its antiproliferative effects. These results align well with prior research on the cytotoxic activity of abietane-type diterpenes possessing a quinone moiety [26]; in this study, the researchers confirmed that the orthoquinone was the critical structural component for cytotoxicity in abietane diterpenoids with a naphthalene quinone moiety. They also demonstrated that tebesinone B and aegyptinone A (5.47–10.34 and 2.11–8.19 µM, respectively) as orthoquinones possessed higher activity than tebesinone A and aegyptinone B as para-quinones. Some other studies have also mentioned how drastically the cytotoxic activity of rearranged abietane diterpenes increases from the para to the ortho-orientation [27–30]. In addition, other research indicated the potent cytotoxic effect, against human carcinoma KB cells, of an orthoquinone-rearranged abietane, aethiopinone, whose structure is very close to that of saprorthoquinone (**7**) [31]. Significant cytotoxicity of aethiopinone has been demonstrated in other studies against human leukemia lymphoblastic NALM-6 (IC_{50} = 0.6 µg/mL) and promyelocytic HL-60 cells (IC_{50} = 4.8 µg/mL) [32].

Among the diterpenoids obtained in this study, pygmaeocin B (**5**), a rearranged abietane-type diterpenoid with an orthoquinone group on the C-ring, showed potent activity against human colon adenocarcinoma cells (HT29) and hepatocarcinoma tumor cells (HepG2). In contrast, viridoquinone did not display significant cytotoxicity in these cell lines, suggesting that the carbonyl group at the C2 position of pygmaeocin B plays a crucial role in enhancing the reactivity of the orthoquinone group (Figure 1). Additionally, another compound, saprorthoquinone (**7**), containing an orthoquinone moiety, exhibited significant cytotoxic effects against HT29 and murine melanoma cells (B16–F10). Other saprorthoquinone derivatives with biological properties have been described. In this context, a recent study showed the discovery of novel derivatives of saprorthoquinone (**7**) isolated from Salvia prionitis Hance, with dual inhibitor properties of Indoleamine 2,3-Dioxygenase 1 (IDO1) and Histone Deacetylase 1 (HDAC1). These results demonstrate that the orthoquinone moiety is a key pharmacophore for IDO1 and HDAC1 inhibition, providing a potential strategy for cancer treatment by exploiting both immunotherapeutic and epigenetic drugs [33]. Moreover, pygmaeocin C (**17**) with a catechol moiety that can be easily oxidized to form an orthoquinone showed decreased activity compared with pygmaeocin B (**5**). At the cellular level, orthoquinones can be enzymatically reduced by cytochrome P450, generating reactive oxygen species (ROS) capable of damaging the DNA and proteins of tumor cells [34], thus explaining the greater cytotoxicity observed in pygmaeocin B (**5**) (Figure 1).

The discovery and development of cytotoxic compounds with the ability to inhibit cell growth through cell cycle arrest and induction of apoptosis have been of great interest in

the field of anti-cancer drug discovery [35–39]. In this study, two compounds, orthoquinone (**13**) and pygmaeocin B (**5**), were evaluated for their antiproliferative activity against the HT29 colon adenocarcinoma line. Both compounds showed significant antiproliferative effects, with pygmaeocin B (**5**) exhibiting greater potency. The mechanism of action of these compounds involves cell cycle arrest in the S phase and the induction of apoptosis, similar to other abietanes and related diterpenoids studied previously, such as tanshinone IIA [40] and triptolide [41].

Furthermore, apoptosis studies by AnnexinV-Fict staining together with mitochondrial membrane potential studies by Rhodamine 123 staining demonstrated that both compounds **5** and **13** induced apoptosis through the intrinsic apoptotic pathway at remarkably low concentrations, leading to a significant inhibition of HT29 cell viability. In addition, both compounds induced morphological changes characteristic of apoptosis, such as chromatin condensation and fragmentation, as evidenced by fluorescence microscopy. These findings agree with previous studies showing that some naturally occurring abietane diterpenes appear to induce apoptosis via the intrinsic pathway. For example, 6, 7-dehydroroyleanone [42] and rosmanol [43] were found to activate caspases 3 and 9, indicating their ability to induce apoptosis through the intrinsic cell death pathway. Therefore, further investigations are necessary to fully elucidate the mechanism responsible for the apoptotic effect of pygmaeocin B (**5**) and its precursor **13**.

Inflammation is a natural innate process of the immune system. However, when it persists for a prolonged period, it can trigger various chronic diseases including cancer [23]. The close relationship between colorectal cancer and the inflammatory state [44] prompted the analysis of the anti-inflammatory activity of the rearranged abietanes under study. According to the results, pygmaeocin B (**5**), with proapoptotic action against colon cancer cells, exhibited the highest anti-inflammatory activity. It inhibited NO production by the RAW 264.7 macrophage line at an extremely low $IC_{50\,NO}$ value. Orthoquinones **13**, **7**, and **19** and catechol quinone **17** followed pygmaeocin B (T) in terms of inhibition.

Previous studies have indicated that the inhibition of orthoquinone tanshinones abietanes diterpenes, including tanshinone IIA and cryptotanshinone, may decrease prostaglandin (PGE2) production via microsomal prostaglandin E2 synthase (mPGES-1), indicating a potential connection with their antiinflammatory and antiplatelet activities [45]. The immunomodulatory effects of abietanes paraquinone derivatives from the roots of Horminum pyrenaicum have been described; the extract fraction containing diterpene quinones horminones, specifically 15, 16-dehydroinuroyleanol, showed the most significant antiinflammatory effect on human peripheral blood mononuclear cells (PBMC) activated by phytohaemagglutinin [46].

Regarding the catechol group, nor-abietane diterpenoids extracted from Perovskia abrotanoides roots have shown great potential as anti-inflammatory agents, specifically catechol: deoxy-1,2-dien-3-oxoarucadio inhibited iNOS expression and NO production in LPS-stimulated J774A.1 macrophages [47].

Human cancer is a very complex disease, and therefore, more multifunctional drugs need to be developed. Efforts are needed to redirect research toward this goal. For example, the signaling pathway of the transcription factor NF-kβ is crucial to the interconnection between colorectal cancer and the inflammatory state, causing the activation of both proinflammatory and tumorigenesis-related genes. Furthermore, it highlights the role of the antiapoptotic members of the Blc-2 protein family [44]. NFkβ becomes a crucial therapeutic target to prevent and treat colorectal cancer. In future studies, it would be interesting to verify if pygmaeocin B (**5**) and other studied abietanes and rearranged abietanes exhibit a dual action through inhibition.

4. Materials and Methods

4.1. Chemistry

Experimental Procedures

The experimental procedure for the synthesis of compounds **5**, **13**, **14**, **15**, **16**, **17**, **18**, **19**, and **21** was previously described by our research group [21]. The experimental procedures for the synthesis of compounds **7**, **12**, and **20** and the ^{1}H and ^{13}C NMR spectra are included in the Supplementary Materials (see Tables S1 and S2).

4.2. Biological Experimental Procedures

4.2.1. Materials

Dulbecco's modified Eagle medium (DMEM), RPMI 1640 W/L-Glutamine, fetal bovine serum (FBS), penicillin/streptomycin (Biowest, Nuaillé, France), gentamicin (Biowest, Nuaillé, France), dimethylsulfoxide (DMSO, Merck Life Science S.L., Madrid, Spain), and 3-(4,5-dimethylthiazol-2-yl)-2,5-diphenyltetrazolium bromide (MTT) were purchased from Thermo Fisher Scientific Inc. (Ward Hill, MA, USA). Culture flasks and well plates were obtained from VWR International Ltd. (Radnor, PA, USA).

4.2.2. Test Compounds

Firstly, the compounds (**5**, **7**, **13**, **17**, and **19**) were dissolved in DMSO at 5 mg/mL. Stock solution was stored at -20 °C before treatment and diluted in cell culture medium to appropriate concentrations for each experiment. For the antiproliferative assay in all cell lines, we determined the concentrations of compounds required for 20, 50, and 80% inhibition of cell growth, IC_{20}, IC_{50}, and IC_{80}, concentrations, respectively, to analyze the full range of cytotoxicity and to determine the graded or acute response to these compounds. Subcytotoxic concentrations ($\frac{3}{4}$ IC_{50}, $\frac{1}{2}$ IC_{50}, and $\frac{1}{4}$ IC_{50}), were used for the nitrite assay. All experiments were measured and compared with untreated control cells.

4.2.3. Cell Culture and Viability Assay

The human colorectal adenocarcinoma cell line HT29 (ECACC no. 9172201; ATCC no. HTB-38), the human hepatocarcinoma cell line HepG2 (ECACC no. 85011430), the mouse melanoma cells B16–F10 (ATCC no. CRL-6475), and the murine monocyte/macrophage like RAW 264.7 cell line (ATCC no, TIB-71) were obtained from the cell bank of the University of Granada, Spain. The tumor cell lines were cultured in DMEM (Dulbecco's modified Eagle's medium) supplemented with 2 mM glutamine, 10% heat-inactivated FCS (fetal calf serum), and 50 μg/mL of gentamicin (for all cancer cell lines). The RAW 264.7 cell line was cultured in RPMI1640 medium, supplemented with 2 mM glutamine, 10% heat-inactivated FCS, and 50 μg/mL of gentamicin. All cell lines were incubated at 37 °C, in an atmosphere of 5% CO_2 and 95% humidity. The culture media were changed every 48 h, and the confluent cultures were separated with a trypsin solution (0.25% EDTA). In all experiments, monolayer cells were grown to 80–90% confluence in sterile cell culture flasks.

The effects of the compounds on the cell viability were established using the MTT method [48] (Sigma, St. Louis, MO, USA). The cytotoxicity of the compounds was assessed by measuring the absorbance of MTT dye staining of metabolically competent cells. The cells were cultivated in 96-well plates at 6.0×10^3 cells/mL for the HT29 and RAW 264.7 cell lines, at 5.0×10^3 cells/mL for B16–F10 cells, and 15.0×10^3 cells/mL for the HepG2 cell line, with a final volume of 200 μL per well being incubated with the different products (0–100 μg/mL). After 72 h, 100 μL of MTT solution (0.5 mg/mL) in 50% of PBS and 50% of the medium was added to each well. Following incubation for 1.5 h, formazan was resuspended in 100 μL of DMSO, and each concentration was tested in triplicate. The cell viability relative to the untreated control cells was determined by measuring the absorbance at 570 nm using an ELISA plate reader (Tecan Sunrise MR20–301, TECAN, Grödig, Austria). Compounds that had low IC_{50} values (5 and 13) were chosen for multiple cytometry assays, including the determination of apoptosis, cell cycle, and mitochondrial membrane potential determination.

4.2.4. Measurement of Nitric Oxide Concentration

Nitrite production was analyzed using the Griess reaction method. The concentration of nitrite was used as an indication of nitric oxide (NO) production [49]. RAW 264.7 cells were seeded at 6×10^4 cells/well in 24-well cell culture plates, supplemented with 10 µg/mL of lipopolysaccharide (LPS). After 24 h, the cells were treated with compounds (**5**, **7**, **13**, **17**, and **19**) at concentrations equivalent to ¾ IC_{50}, ½ IC_{50}, and ¼ IC_{50} of their half-maximal inhibitory concentration (IC_{50}) for 48 h. The Griess reaction [50] was conducted by mixing 150 µL of supernatant test samples or sodium nitrite standard (0–120 µM) with 25 µL of Griess reagent A (0.1% n-(1-naphthyl) ethylenediamine dihydrochloride) and 25 µL of Griess reagent B (1% sulfanilamide in 5% of phosphoric acid) in a 96-well plate. The mixture was incubated at room temperature for 15 min, after which the absorbance was measured at 540 nm using an ELISA plate reader (Tecan Sunrise MR20–301, TECAN, Grödig, Austria). To determine the concentration of nitrite in each sample supernatant, the absorbance was referenced to the nitrite standard curve. To determine the percentage of NO production, the increase between the negative control (untreated cells) and the positive control (cells only with 10 µg/mL of LPS) was assigned 100%.

4.2.5. HT29 Cell Cycle Analysis

The amount of DNA in the different phases of the cell cycle (G0/G1, S, and G2/M) was quantified using flow cytometry after staining with propidium iodide (PI) [51]. HT29 cells were seeded at a density of 5×10^4 cells per well in 24-well plates containing 1.5 mL of culture medium. After 24 h the cells were treated with IC_{50} and IC_{80} concentrations of compounds **5** and **13** for 72 h. Next, the cells were washed twice with PBS, trypsinized, and resuspended in $1 \times$ TBS (10 mM Tris and 150 mM NaCl). After this, Vindelov buffer (100 mM Tris, 100 mM NaCl, 10 mg/mL Rnase, 1 mg/mL PI, and 0.1% Triton x-100, pH 8) was added. Finally, the cells were kept on ice and stained with 20 µL of 1 mg/mL PI solution before being measured. Each experiment analyzed approximately 10×10^3 cells. The experiments were performed twice, each with three replications per assay. The samples were analyzed using a flow cytometer, and the number of cells in each stage of the cell cycle was estimated by fluorescence-associated cell sorting (FACS) at 488 nm in an Epics XL flow cytometer (Coulter Corporation, Hialeah, FL, USA).

4.2.6. Annexin V-FITC/Propidium Iodide Flow Cytometry Analysis

Flow cytometry was used to detect annexin V-FICT and PI double staining, to quantify the pro-apoptotic impact of compounds **5** and **13**. Apoptosis was assessed through flow cytometry using a FACScan flow cytometer (Coulter Corporation, Hialeah, FL, USA). In this assay, 5×10^4 HT29 cells were plated in 24-well plates with 1.5 mL of medium and incubated for 24 h. The cells were then treated with the selected compounds in triplicate for 24, 48, and 72 h at their corresponding IC_{50} and IC_{80} concentrations. The cells were harvested and resuspended in a binding buffer (10 mM HEPES/NaOH with pH 7.4, 140 mM NaCl, and 2.5 mM $CaCl_2$). Subsequently, Annexin V-FITC conjugate (1 µg/mL) was added and incubated for 15 min in the dark at room temperature. The cells were stained with 5 µL of 1 mg/mL PI solution before analysis. Approximately 10×10^3 cells were analyzed in each experiment; the experiments were performed twice, each with three replications per assay.

4.2.7. Flow Cytometry Analysis of the Mitochondrial Membrane Potential

We analyzed the electrochemical gradient across the mitochondrial membrane via analytical flow cytometry, using dihydrorhodamine (DHR). A total of 5×10^4 HT29 cells were plated in 24-well plates for this assay. These cells were incubated for 24 h and then treated with compounds **5** and **13** at their corresponding IC_{50} and IC_{80} concentrations for 48 h. Next, the medium was replaced by adding fresh solution with DHR to a final concentration of 5 µg/mL. The cells were incubated at 37 °C for 1 h, washed, and resuspended in PBS with 5 µg/mL of PI. The fluorescence intensity was measured using a FACScan flow

cytometer (fluorescence-activated cell sorter). The experiments were performed two times, each with three replications per assay.

4.2.8. Hoechst-Stained Fluorescence Microscopy

The morphological changes were analyzed using Hoechst-stained fluorescence microscopy. For the analysis, 15×10^4 HT29 cells were plated on a coverslip within a 24-well plate. After 24 h, compounds **5** and **13** were added to the cells and incubated at their respective IC_{50} and IC_{80} concentrations for the next 72 h. The cells were washed twice with PBS, treated with cold MeOH for 3 min, washed again with PBS, and then incubated in 500 µL of Hoechst solution (50 ng/mL) in PBS for 15 min in the dark. Finally, the samples were visualized through fluorescent microscopy (DMRB, Leica Microsystems, Wetzlar, Germany) under a DAPI filter.

4.2.9. Statistical Analysis

The data were represented as the mean $\pm$ standard deviation (SD). For each experiment, the Student's *t* test was used for statistical comparisons against the untreated control cells. A limit of $p < 0.05$ was used to determine the significant differences. $p < 0.05$ (*), $p < 0.01$ (**), and $p < 0.001$ (***). All data shown here were representative of at least two independent experiments, performed in triplicate.

5. Conclusions

In conclusion, the synthesis of some rearranged abietanes was carried out, including the synthesis of saprorthoquinone (**7**) and the first synthesis of 1-deoxyviroxocin (**12**) confirming its structure. Our biological study demonstrated the anti-inflammatory potential power of these compounds, especially the rearranged abietane pygmaeocin B (**5**) and its precursor orthoquinone **13**, Pygmaeocin C (**17**), and Viridoquinone (**19**), with very low IC_{50NO} values in (LPS)-induced RAW 264.7 cells. We also demonstrated the high anticancer potential of these compounds, especially of compounds **5** and **13**, in HT29 colon cancer cells with very low values of IC_{50} and with clear activation of apoptosis and intrinsic apoptotic pathway activation, as the results of apoptosis, cell cycle, and mitochondrial mem-brane potential have shown. The investigation of diterpenoids provided valuable insights into their cytotoxic and anti-cancer properties. These findings reveal the bioactive potential of the rearranged abietanes group for the first time, providing valuable knowledge to conduct further research of these natural products with respect to their anti-inflammatory and anticancer activities and, thus, study their detailed molecular mechanisms.

References

1. Song, M.; Giovannucci, E. Preventable incidence and mortality of carcinoma associated with lifestyle factors among white adults in the United States. *JAMA Oncol.* **2016**, *2*, 1154–1161. [CrossRef]
2. Huang, M.; Lu, J.-J.; Ding, J. Natural Products in Cancer Therapy: Past, Present and Future. *Nat. Prod. Bioprospect.* **2021**, *11*, 5–13. [CrossRef] [PubMed]
3. Newman, D.J.; Cragg, G.M. Natural Products as Sources of New Drugs over the 30 Years from 1981 to 2010. *J. Nat. Prod.* **2012**, *75*, 311–335. [CrossRef]
4. Yang, L.; Wen, K.-S.; Ruan, X.; Zhao, Y.-X.; Wei, F.; Wang, Q. Response of Plant Secondary Metabolites to Environmental Factors. *Molecules* **2018**, *23*, 762. [CrossRef] [PubMed]
5. Kang, J.; Le, T.Q.; Oh, C.H. Recent Advances in Abietane/Icetexane Synthesis. *Tetrahedron* **2022**, *108*, 154133. [CrossRef]
6. Nagata, H.; Miyazawa, N.; Ogasawara, K. Tandem Single-Step Construction of Chiral Hexahydrophenanthrenes: A Concise Route to (+)-Ferruginol. *Org. Lett.* **2001**, *3*, 1737–1740. [CrossRef]
7. Lv, C.; Zeng, H.-W.; Wang, J.-X.; Yuan, X.; Zhang, C.; Fang, T.; Yang, P.-M.; Wu, T.; Zhou, Y.-D.; Nagle, D.G.; et al. The Antitumor Natural Product Tanshinone IIA Inhibits Protein Kinase C and Acts Synergistically with 17-AAG. *Cell Death Dis.* **2018**, *9*, 165. [CrossRef]
8. Furman, D.; Campisi, J.; Verdin, E.; Carrera-Bastos, P.; Targ, S.; Franceschi, C.; Ferrucci, L.; Gilroy, D.W.; Fasano, A.; Miller, G.W.; et al. Chronic inflammation in the etiology of disease across the life span. *Nat. Med.* **2019**, *25*, 1822–1832. [CrossRef]
9. Zappavigna, S.; Cossu, A.M.; Grimaldi, A.; Bocchetti, M.; Ferraro, G.A.; Nicoletti, G.F.; Filosa, R.; Caraglia, M. Anti-inflammatory drugs as anticancer agents. *Int. J. Mol. Sci.* **2020**, *21*, 2605. [CrossRef]
10. Galisteo, A.; Jannus, F.; García-García, A.; Aheget, H.; Rojas, S.; Lupiañez, J.A.; Rodríguez-Diéguez, A.; Reyes-Zurita, F.J.; Quílez del Moral, J.F. Diclofenac N-derivatives as therapeutic agents with anti-inflammatory and anti-cancer effect. *Inter. J. Mol. Sci.* **2021**, *22*, 5067. [CrossRef] [PubMed]
11. Lin, W.-H.; Fang, J.-M.; Cheng, Y.-S. Diterpenes and Related Cycloadducts from Taiwania cryptomerioides. *Phytochemistry* **1996**, *42*, 1657–1663. [CrossRef]
12. Majetich, G.; Zou, G. Total Synthesis of (−)-Barbatusol, (+)-Demethylsalvicanol, (−)-Brussonol, and (+)-Grandione. *Org. Lett.* **2008**, *10*, 81–83. [CrossRef]
13. Chen, W.; Meng, Q.; Piantini, U.; Hesse, M. Two Novel Diterpenoids from Pygmaeopremna herbacea. *J. Nat. Prod.* **1989**, *52*, 581–587. [CrossRef]
14. Monache, F.D.; Monache, G.D.; Gacs-Baitz, E.; De Coelho, J.S.; De Albuquerque, I.L.; De Chiappeta, A.; De Mello, J.F. Um-brosone, An Ortho-Quinone from Hyptis umbrosa. *Phytochemistry* **1990**, *29*, 3971–3972. [CrossRef]
15. Lin, L.-Z.; Blaskó, G.; Cordell, G.A. Diterpenes of *Salvia prionitis*. *Phytochemistry* **1989**, *28*, 177–181. [CrossRef]
16. Ulubelen, A.; Topçu, G.; Chai, H.-B.; Pezzuto, J.M. Cytotoxic Activity of Diterpenoids Isolated from *Salvia hypargeia*. *Pharm. Biol.* **1999**, *37*, 148–151. [CrossRef]
17. Naman, C.B.; Gromovsky, A.D.; Vela, C.M.; Fletcher, J.N.; Gupta, G.; Varikuti, S.; Zhu, X.; Zywot, M.; Chai, H.; Werbovetz, K.A.; et al. Antileishmanial and Cytotoxic Activity of Some Highly Oxidized Abietane Diterpenoids from the Bald Cypress, Taxodium distichum. *J. Nat. Prod.* **2016**, *79*, 598–606. [CrossRef] [PubMed]
18. Xia, F.; Luo, D.; Wang, T.; Ji, X.; Xu, G. Vasorelaxant 4,5-Seco-Abietane Diterpenoids with Diverse 6/6/6, 6/6/7, and 6/6/8 Architectures from *Salvia prattii* Hemsl. *Fitoterapia* **2020**, *142*, 104521. [CrossRef]
19. Zadali, R.; Nejad-Ebrahimi, S.; Hadjiakhoondi, A.; Fiengo, L.; D'Ambola, M.; De Vita, S.; Tofighi, Z.; Chini, M.G.; Bifulco, G.; De Tommasi, N. Diterpenoids from *Zhumeria majdae* Roots as Potential Heat Shock Protein 90 (HSP90) Modulators. *Phytochemistry* **2021**, *185*, 112685. [CrossRef]
20. Zhao, S.-M.; Chou, G.-X.; Yang, Q.-S.; Wang, W.; Zhou, J.-L. Abietane Diterpenoids from Caryopteris incana (Thunb.) Miq. *Org. Biomol. Chem.* **2016**, *14*, 3510–3511. [CrossRef]
21. Ait El Had, M.; Guardia, J.J.; Ramos, J.M.; Taourirte, M.; Chahboun, R.; Alvarez-Manzaneda, E. Bioinspired Synthesis of Pygmaeocins and Related Rearranged Abietane Diterpenes: Synthesis of Viridoquinone. *Org. Lett.* **2018**, *20*, 5666–5670. [CrossRef] [PubMed]
22. Matsumoto, T.; Tanaka, Y.; Terao, H.; Takeda, Y.; Wada, M. The Synthesis of Salvinolone, Saprorthoquinone, and 4-Hydroxysapriparaquinone from (+)-Dehydroabietic Acid. *Bull. Chem. Soc. Jpn.* **1993**, *66*, 3053–3057. [CrossRef]
23. Jannus, F.; Medina-O'Donnell, M.; Rivas, F.; Díaz-Ruiz, L.; Rufino-Palomares, E.E.; Lupiáñez, J.A.; Parra, A.; Reyes-Zurita, F.J. A diamine-PEGylated oleanolic acid derivative induced efficient apoptosis through a death receptor and mitochondrial apoptotic pathway in HepG2 human hepatoma cells. *Biomolecules* **2020**, *10*, 1375. [CrossRef] [PubMed]
24. González, M.A. Aromatic abietane diterpenoids: Their biological activity and synthesis. *Nat. Prod. Rep.* **2015**, *32*, 684–704. [CrossRef]
25. Kuroda, Y.; Nicacio, K.J.; da Silva, I.A., Jr.; Leger, P.R.; Chang, S.; Gubiani, J.R.; Deflon, V.M.; Nagashima, N.; Rode, A.; Blackford, K.; et al. Isolation, synthesis and bioactivity studies of phomactin terpenoids. *Nat. Chem.* **2018**, *10*, 938–945. [CrossRef]
26. Eghbaliferiz, S.; Emami, S.A.; Tayarani-Najaran, Z.; Iranshahi, M.; Shakeri, A.; Hohmann, J.; Asili, J. Cytotoxic diterpene quinones from *Salvia tebesana* Bunge. *Fitoterapia* **2018**, *128*, 97–101. [CrossRef] [PubMed]
27. Chang, J.; Xu, J.; Li, M.; Zhao, M.; Ding, J.; Zhang, J.S. Novel cytotoxic seco-abietane rearranged diterpenoids from *Salvia prionitis*. *Planta Med.* **2005**, *71*, 861–866. [CrossRef]

28. Zheng, X.; Kadir, A.; Zheng, G.; Jin, P.; Qin, D.; Maiwulanjiang, M.; Aisa, H.A.; Yao, G. Antiproliferative abietane quinone diterpenoids from the roots of *Salvia deserta*. *Bioorg. Chem.* **2020**, *104*, 104261. [CrossRef]

29. Chen, X.; Ding, J.; Ye, Y.M.; Zhang, J.S. Bioactive Abietane and s eco-Abietane Diterpenoids from *Salvia prionitis*. *J. Nat. Prod.* **2002**, *65*, 1016–1020. [CrossRef]

30. Nazemosadat-Arsanjani, Z.; Moein, M.; Yousuf, S.; Firuzi, O.; Choudhary, M.I. Reassessing the molecular structures of some previously isolated abietane diterpenoids with a naphthalene moiety and the structure-activity relationship (SAR) of quinone diterpenoids. *Phytochemistry* **2022**, *204*, 113433. [CrossRef]

31. Hernandez-Perez, M.; Rabanal, R.M.; Arias, A.; de La Torre, M.C.; Rodriguez, B. Aethiopinone, an antibacterial and cytotoxic agent from *Salvia aethiopis* roots. *Pharm. Biol.* **1999**, *37*, 17–21. [CrossRef]

32. Różalski, M.; Kuźma, Ł.; Wysokińska, H.; Krajewska, U. Cytotoxic and proapoptotic activity of diterpenoids from in vitro cultivated *Salvia sclarea* roots. Studies on the leukemia cell lines. *Z. Naturforsch. C J. Biosci.* **2006**, *61*, 483–488. [CrossRef] [PubMed]

33. Lin, Y.; Zhang, H.; Niu, T.; Tang, M.L.; Chang, J. Discovery of novel indoleamine 2, 3-dioxygenase 1 (IDO1) and histone deacetylase 1 (HDAC1) dual inhibitors derived from the natural product saprorthoquinone. *Molecules* **2020**, *25*, 4494. [CrossRef]

34. Netto, C.D.; Santos, E.S.; Castro, C.P.; da Silva, A.J.; Rumjanek, V.M.; Costa, P.R. (±)-3, 4-Dihydroxy-8, 9-methylenedioxypterocarpan and derivatives: Cytotoxic effect on human leukemia cell lines. *Eur. J. Med. Chem.* **2009**, *44*, 920–925. [CrossRef] [PubMed]

35. Barnum, K.J.; O'Connell, M.J. Cell cycle regulation by checkpoints. *Cell Cycle Control Mech. Protoc.* **2014**, *1170*, 29–40.

36. Karunagaran, D.; Rashmi, R.; Kumar, T.R. Induction of apoptosis by curcumin and its implications for cancer therapy. *Curr. Cancer Drug Targets* **2005**, *5*, 117–129. [CrossRef] [PubMed]

37. Tegeder, I.; Grösch, S.; Schmidtko, A.; Häussler, A.; Schmidt, H.; Niederberger, E.; Scholich, K.; Geisslinger, G. G protein-independent G1 cell cycle block and apoptosis with morphine in adenocarcinoma cells: Involvement of p53 phosphorylation. *Cancer Res.* **2003**, *63*, 1846–1852. [PubMed]

38. Senwar, K.R.; Sharma, P.; Reddy, T.S.; Jeengar, M.K.; Nayak, V.L.; Naidu, V.G.; Kamal, A.; Shankaraiah, N. Spirooxindole-derived morpholine-fused-1, 2, 3-triazoles: Design, synthesis, cytotoxicity and apoptosis inducing studies. *Eur. J. Med. Chem.* **2015**, *102*, 413–424. [CrossRef] [PubMed]

39. Zentar, H.; Jannus, F.; Gutierrez, P.; Medina-O'Donnell, M.; Lupiáñez, J.A.; Reyes-Zurita, F.J.; Alvarez-Manzaneda, E.; Chahboun, R. Semisynthesis and Evaluation of Anti-Inflammatory Activity of the Cassane-Type Diterpenoid Taepeenin F and of Some Synthetic Intermediates. *J. Nat. Prod.* **2022**, *85*, 2372–2384. [CrossRef]

40. Xie, J.; Liu, J.; Liu, H.; Liang, S.; Lin, M.; Gu, Y.; Liu, T.; Wang, D.; Ge, H.; Mo, S.L. The antitumor effect of tanshinone IIA on anti-proliferation and decreasing VEGF/VEGFR2 expression on the human non-small cell lung cancer A549 cell line. *Acta Pharm. Sin. B* **2015**, *5*, 554–563. [CrossRef]

41. Hu, Y.P.; Tan, Z.J.; Wu, X.S.; Liu, T.Y.; Jiang, L.; Bao, R.F.; Shu, Y.J.; Li, M.L.; Weng, H.; Ding, Q.; et al. Triptolide induces s phase arrest and apoptosis in gallbladder cancer cells. *Molecules* **2014**, *19*, 2612–2628. [CrossRef] [PubMed]

42. Garcia, C.; Silva, C.O.; Monteiro, C.M.; Nicolai, M.; Viana, A.; Andrade, J.M.; Barasoain, I.; Stankovic, T.; Quintana, J.; Hernández, I.; et al. Anticancer properties of the abietane diterpene 6, 7-dehydroroyleanone obtained by optimized extraction. *Future Med. Chem.* **2018**, *10*, 1177–1189. [CrossRef]

43. Cheng, A.C.; Lee, M.F.; Tsai, M.L.; Lai, C.S.; Lee, J.H.; Ho, C.T.; Pan, M.H. Rosmanol potently induces apoptosis through both the mitochondrial apoptotic pathway and death receptor pathway in human colon adenocarcinoma COLO 205 cells. *Food Chem. Toxicol.* **2011**, *49*, 485–493. [CrossRef] [PubMed]

44. Terzić, J.; Grivennikov, S.; Karin, E.; Karin, M. Inflammation and colon cancer. *Gastroenterology* **2010**, *138*, 2101–2114. [CrossRef]

45. Maione, F.; Cantone, V.; Chini, M.G.; De Feo, V.; Mascolo, N.; Bifulco, G. Molecular mechanism of tanshinone IIA and cryptotanshinone in platelet anti-aggregating effects: An integrated study of pharmacology and computational analysis. *Fitoterapia* **2015**, *100*, 174–178. [CrossRef]

46. Becker, K.; Schwaiger, S.; Waltenberger, B.; Fuchs, D.; Pezzei, C.K.; Schennach, H.; Stuppner, H.; Gostner, J.M. Immunomodulatory effects of diterpene quinone derivatives from the roots of Horminum pyrenaicum in human PBMC. *Oxid. Med. Cell Longev.* **2018**, *2018*, 2018. [CrossRef]

47. Alizadeh, Z.; Farimani, M.M.; Parisi, V.; Marzocco, S.; Ebrahimi, S.N.; De Tommasi, N. Nor-abietane diterpenoids from Perovskia abrotanoides roots with anti-inflammatory potential. *J. Nat. Prod.* **2021**, *84*, 1185–1197. [CrossRef]

48. Mosmann, T. Rapid colorimetric assay for cellular growth and survival: Application to proliferation and cytotoxicity assays. *J. Immunol. Methods* **1983**, *65*, 55–63. [CrossRef] [PubMed]

49. Connelly, L.; Palacios-Callender, M.; Ameixa, C.; Moncada, S.; Hobbs, A.J. Biphasic regulation of NF-κB activity underlies the pro-and anti-inflammatory actions of nitric oxide. *J. Immunol.* **2001**, *166*, 3873–3881. [CrossRef]

50. Bryan, N.S.; Grisham, M.B. Methods to Detect Nitric Oxide and Its Metabolites in Biological Samples. *Free Radic. Biol. Med.* **2007**, *43*, 645–657. [CrossRef]

51. Vega-Granados, K.; Medina-O'Donnell, M.; Rivas, F.; Reyes-Zurita, F.J.; Martinez, A.; Alvarez de Cienfuegos, L.; Lupiañez, J.A.; Parra, A. Synthesis and biological activity of triterpene–coumarin conjugates. *J. Nat. Prod.* **2021**, *84*, 1587–1597. [CrossRef] [PubMed]